Solar water heating and vaporization with silicon nanoparticles at mie resonances

Satoshi Ishii,[1,2,*] Ramu Pasupathi Sugavaneshwar,[1,2] Kai Chen,[1,2] Thang Duy Dao[1,2] and Tadaaki Nagao[1,2]

[1] *International Center for Materials Nanoarchitectonics (MANA), National Institute for Materials Science (NIMS), Tsukuba, Ibaraki 305-0044, Japan*
[2] *CREST, Japan Science and Technology Agency, Kawaguchi, Saitama 332-0012, Japan*
[*] *sishii@nims.go.jp*

Abstract: We propose analytically and demonstrate experimentally that an ensemble of silicon nanoparticles with different sizes can effectively absorb sunlight. Due to the extinction of silicon from UV to near-infrared region, Mie resonances in silicon nanoparticles dramatically enhance the absorption of solar light. In experiment, silicon nanoparticles dispersed in water worked as excellent sunlight-heat transducers that efficiently harvest sunlight to accelerate heating and vaporization of water by nanoscale local heating. Our study opens up the potential of silicon nanoparticles in various solar-thermal applications.

OCIS codes: (290.4020) Mie theory; (350.5340) Photothermal effects; (260.5740) Resonance; (160.4236) Nanomaterials; (160.6000) Semiconductor materials.

References and links

1. H. Tyagi, P. Phelan, and R. Prasher, "Predicted efficiency of a nanofluid-based direct absorption solar receiver," in *ASME 2007 Energy Sustainability Conference* (American Society of Mechanical Engineers, Long Beach, CA, USA, 2007), pp. 729–736.
2. T. P. Otanicar and J. S. Golden, "Comparative environmental and economic analysis of conventional and nanofluid solar hot water technologies," Environ. Sci. Technol. **43**(15), 6082–6087 (2009).
3. R. A. Taylor, P. E. Phelan, T. P. Otanicar, C. A. Walker, M. Nguyen, S. Trimble, and R. Prasher, "Applicability of nanofluids in high flux solar collectors," J. Renewable Sustainable Energy **3**(2), 023104 (2011).
4. R. A. Taylor, T. Otanicar, and G. Rosengarten, "Nanofluid-based optical filter optimization for PV/T systems," Light Sci. Appl. **1**(10), e34 (2012).
5. O. Mahian, A. Kianifar, S. A. Kalogirou, I. Pop, and S. Wongwises, "A review of the applications of nanofluids in solar energy," Int. J. Heat Mass Transfer **57**(2), 582–594 (2013).
6. C. Li, Y. Liu, X. Huang, and H. Jiang, "Direct Sun-Driven Artificial Heliotropism for Solar Energy Harvesting Based on a Photo-Thermomechanical Liquid-Crystal Elastomer Nanocomposite," Adv. Funct. Mater. **22**(24), 5166–5174 (2012).
7. D. Han, Z. Meng, D. Wu, C. Zhang, and H. Zhu, "Thermal properties of carbon black aqueous nanofluids for solar absorption," Nanoscale Res. Lett. **6**(1), 457 (2011).
8. L. Mercatelli, E. Sani, G. Zaccanti, F. Martelli, P. Di Ninni, S. Barison, C. Pagura, F. Agresti, and D. Jafrancesco, "Absorption and scattering properties of carbon nanohorn-based nanofluids for direct sunlight absorbers," Nanoscale Res. Lett. **6**(1), 282 (2011).
9. H. Ghasemi, G. Ni, A. M. Marconnet, J. Loomis, S. Yerci, N. Miljkovic, and G. Chen, "Solar steam generation by heat localization," Nat. Commun. **5**, 4449 (2014).
10. Y. Ito, Y. Tanabe, J. Han, T. Fujita, K. Tanigaki, and M. Chen, "Multifunctional Porous Graphene for High-Efficiency Steam Generation by Heat Localization," Adv. Mater. **27**(29), 4302–4307 (2015).
11. H. Chen, L. Shao, T. Ming, Z. Sun, C. Zhao, B. Yang, and J. Wang, "Understanding the Photothermal Conversion Efficiency of Gold Nanocrystals," Small **6**(20), 2272–2280 (2010).
12. G. Baffou and R. Quidant, "Thermo-plasmonics: using metallic nanostructures as nano-sources of heat," Laser Photonics Rev. **7**(2), 171–187 (2013).
13. C. Loo, A. Lin, L. Hirsch, M.-H. Lee, J. Barton, N. Halas, J. West, and R. Drezek, "Nanoshell-enabled photonics-based imaging and therapy of cancer," Technol. Cancer Res. Treat. **3**(1), 33–40 (2004).
14. G. L. Liu, J. Kim, Y. Lu, and L. P. Lee, "Optofluidic control using photothermal nanoparticles," Nat. Mater. **5**(1), 27–32 (2006).
15. X.-M. Zhu, C. Fang, H. Jia, Y. Huang, C. H. Cheng, C.-H. Ko, Z. Chen, J. Wang, and Y.-X. J. Wang, "Cellular uptake behaviour, photothermal therapy performance, and cytotoxicity of gold nanorods with various coatings," Nanoscale **6**(19), 11462–11472 (2014).

#253755 Received 10 Nov 2015; revised 22 Dec 2015; accepted 17 Jan 2016; published 27 Jan 2016

16. E. Y. Lukianova-Hleb and D. O. Lapotko, "Influence of transient environmental photothermal effects on optical scattering by gold nanoparticles," Nano Lett. **9**(5), 2160–2166 (2009).
17. R. A. Taylor, P. E. Phelan, T. Otanicar, R. J. Adrian, and R. S. Prasher, "Vapor generation in a nanoparticle liquid suspension using a focused, continuous laser," Appl. Phys. Lett. **95**(16), 161907 (2009).
18. S. Hashimoto, D. Werner, and T. Uwada, "Studies on the interaction of pulsed lasers with plasmonic gold nanoparticles toward light manipulation, heat management, and nanofabrication," J. Photochem. Photobiol. **13**(1), 28–54 (2012).
19. A. Siems, S. Weber, J. Boneberg, and A. Plech, "Thermodynamics of nanosecond nanobubble formation at laser-excited metal nanoparticles," New J. Phys. **13**(4), 043018 (2011).
20. Z. Fang, Y.-R. Zhen, O. Neumann, A. Polman, F. J. García de Abajo, P. Nordlander, and N. J. Halas, "Evolution of light-induced vapor generation at a liquid-immersed metallic nanoparticle," Nano Lett. **13**(4), 1736–1742 (2013).
21. S. Person, M. Jain, Z. Lapin, J. J. Sáenz, G. Wicks, and L. Novotny, "Demonstration of zero optical backscattering from single nanoparticles," Nano Lett. **13**(4), 1806–1809 (2013).
22. L. Cao, D. N. Barsic, A. R. Guichard, and M. L. Brongersma, "Plasmon-Assisted Local Temperature Control to Pattern Individual Semiconductor Nanowires and Carbon Nanotubes," Nano Lett. **7**(11), 3523–3527 (2007).
23. M. Xiao, R. Jiang, F. Wang, C. Fang, J. Wang, and J. C. Yu, "Plasmon-enhanced chemical reactions," J. Mater. Chem. A Mater. Energy Sustain. **1**(19), 5790–5805 (2013).
24. O. Neumann, A. S. Urban, J. Day, S. Lal, P. Nordlander, and N. J. Halas, "Solar vapor generation enabled by nanoparticles," ACS Nano **7**(1), 42–49 (2013).
25. O. Neumann, C. Feronti, A. D. Neumann, A. Dong, K. Schell, B. Lu, E. Kim, M. Quinn, S. Thompson, N. Grady, P. Nordlander, M. Oden, and N. J. Halas, "Compact solar autoclave based on steam generation using broadband light-harvesting nanoparticles," Proc. Natl. Acad. Sci. U.S.A. **110**(29), 11677–11681 (2013).
26. Y. Liu, S. Yu, R. Feng, A. Bernard, Y. Liu, Y. Zhang, H. Duan, W. Shang, P. Tao, C. Song, and T. Deng, "A Bioinspired, Reusable, Paper-Based System for High-Performance Large-Scale Evaporation," Adv. Mater. **27**(17), 2768–2774 (2015).
27. E. D. Palik, *Handbook of Optical Constants of Solids* (Academic Press, 1998), Vol. 3.
28. A. B. Evlyukhin, S. M. Novikov, U. Zywietz, R. L. Eriksen, C. Reinhardt, S. I. Bozhevolnyi, and B. N. Chichkov, "Demonstration of magnetic dipole resonances of dielectric nanospheres in the visible region," Nano Lett. **12**(7), 3749–3755 (2012).
29. Y. H. Fu, A. I. Kuznetsov, A. E. Miroshnichenko, Y. F. Yu, and B. Luk'yanchuk, "Directional visible light scattering by silicon nanoparticles," Nat. Commun. **4**, 1527 (2013).
30. A. I. Kuznetsov, A. E. Miroshnichenko, Y. H. Fu, J. Zhang, and B. Luk'yanchuk, "Magnetic light," Sci. Rep. **2**, 492 (2012).
31. L. Cao, P. Fan, E. S. Barnard, A. M. Brown, and M. L. Brongersma, "Tuning the Color of Silicon Nanostructures," Nano Lett. **10**(7), 2649–2654 (2010).
32. S. Regli, J. A. Kelly, A. M. Shukaliak, and J. G. Veinot, "Photothermal response of photoluminescent silicon nanocrystals," J. Phys. Chem. Lett. **3**(13), 1793–1797 (2012).
33. C. F. Bohren and D. R. Huffman, *Absorption and Scattering of Light by Small Particles* (John Wiley & Sons, 2008).
34. G. M. Hale and M. R. Querry, "Optical Constants of Water in the 200-nm to 200-microm Wavelength Region," Appl. Opt. **12**(3), 555–563 (1973).
35. K. Nakamura, "Synthesis of nanoparticles by thermal plasma processing and its applications," Earozoru Kenkyu **29**, 98–103 (2014).
36. M. E. Straumanis and E. Z. Aka, "Lattice Parameters, Coefficients of Thermal Expansion, and Atomic Weights of Purest Silicon and Germanium," J. Appl. Phys. **23**(3), 330–334 (1952).

1. Introduction

The technology to utilize solar energy for a sustainable society is not limited to photovoltaics. Just as a sheet of black paper can get hot by absorbing sunlight, heat generated from sunlight is an important source of clean energy which people can take advantage of. A typical example is a solar water heater which is often placed on top of a roof to collect solar energy for the water heating. Inside the system there are sunlight absorbers such as tubes or panels, which convert solar energy into thermal energy that is then transferred to water.

A more efficient way of water heating is heating through nanoparticles dispersed in water [1–5], which is called nanofluid. In nanofluid nanoparticles are in direct contact to water so the heat generated at nanoparticles transfers directly to the water. To maximaze the use for solar radiation, a sunlight-driven heliotropism [6] is an ideal function to be added.

The composition of nanoparticles determines the efficiency of the nanofluid. While carbon related nanoparticles [7, 8] and nanostructures [9, 10] are obvious choices as black nanomaterials, it is interesting to look into resonating nanoparticles whose absorption cross sections are enlarged. Among different types of resonances, localized surface plasmon resonances can be excited at metallic nanoparticles leading to enormously enhanced near-field

#253755 Received 10 Nov 2015; revised 22 Dec 2015; accepted 17 Jan 2016; published 27 Jan 2016

intensity and consequently heat localization around the nanoparticles [11, 12]. The applications of such plasmonic heating include photothermal imaging [13], optofluidics [14], photothermal therapy [13, 15], nano-bubble generation [16–21] and nano-chemistry [22, 23] just to name a few. Recent studies have also explored plasmonic nanoparticles in nanofluid applications [24–26].

Another class of resonance is Mie resonance excited at non-metallic nanoparticles. In optical range, the refractive indexes of most of dielectrics are within one to two [27], thus most of the dielectric nanoparticles are too small to support even the lowest order Mie resonance. However, there are a number of semiconductors whose refractive indexes are larger than three and silicon is one such semiconductor. Since the refractive index of silicon is larger than 3.5 from UV to near infrared (NIR) regimes [27], Mie resonances can be excited at silicon nanoparticles in those wavelength range [28–31]. It should be noted that silicon is absorptive below ~1100 nm because of the interband transitions. Therefore, similar to the case with plasmonic nanoparticles, the resonances of silicon nanoparticles below this wavelength region are expected to boost the photothermal conversion [32] with Mie resonances.

In this report, we present analytically and experimentally that silicon nanoparticles have strong light absorptions due to lossy Mie resonances, which efficiently heat up the nanoparticles and the surrounding water. Furthermore, silicon nanoparticles with various particle sizes have different resonant wavelengths ranging from UV to NIR covering the majority of solar spectrum. Our experiment demonstrated that silicon nanoparticles can be effectively heated and the water vaporization rates readily doubled compared to pure water by sunlight illumination. Since the volume fraction of nanoparticles in this nanofluid can be small and silicon is one of the most earth-abundant materials, silicon can be an excellent material for nanofluid that can be adopted for large-scale solar-thermal applications in the future [2, 24].

2. Analysis on lossy Mie resonances

We first present the analytically calculated resonant modes on silicon nanospheres based on Mie theory [33]. In our calculation, the complex permittivity of silicon is taken from ref [27]. (shown in Fig. 4, in the Appendix) and the host index is fixed at 1.33 [34], which is the refractive index of water in optical range. Figure 1 shows the absorption efficiencies (Q_{abs}s) of silicon nanospheres with different radii ranging from 30 nm to 110 nm. Absorption efficiency is a dimensionless quantity where the absorption cross section is normalized to the geometrical cross section of the sphere. In general, the silicon nanospheres display two or more peaks on the spectra except 30-nm silicon nanosphere. The resonance peak at the longest wavelength corresponds to the magnetic dipole mode and the next peak is the electric dipole mode. The peaks in even shorter wavelengths are the higher order modes. Scattering efficiencies (scattering cross section divided by the geometrical cross section of the sphere, Q_{scat}s) of the same silicon nanoparticles are presented in Fig. 5 in the Appendix. Comparing Figs. 1(a) and 5, the absorptions are enhanced where there are resonant scatterings as expected.

In order to verify the mode profiles, numerical simulations based on finite element method are performed using commercial software (COMSOL Multiphysics). Figures 1(b) and 1(c), respectively, show the numerically calculated resistive heating (absorption) at the electric and magnetic resonances for a 50-nm radius silicon sphere. The profiles indicate that the absorptions are enhanced by the resonances. The electric field amplitudes at the corresponding resonances are as well shown in Figs. 1(d) and 1(e), clearly indicating the electric and magnetic modes, respectively.

Since the extinction (imaginary part of the complex refractive index) of silicon is not large in the visible and NIR regimes [27] (see Fig. 4 in the Appendix), all the peaks are rather narrow. Nevertheless, some of the absorption efficiency peaks exceed unity in the visible range, which is promising for strong light absorptions at particular wavelengths. In addition, silicon nanoparticles composed of different sizes can have a broad absorption spectrum as can be anticipated from Fig. 1(a). In the following experimental section, we show that size

#253755 Received 10 Nov 2015; revised 22 Dec 2015; accepted 17 Jan 2016; published 27 Jan 2016

distribution of nanoparticles is indeed advantageous for broadband light absorption from UV to NIR covering more than 70 percent of the solar spectrum.

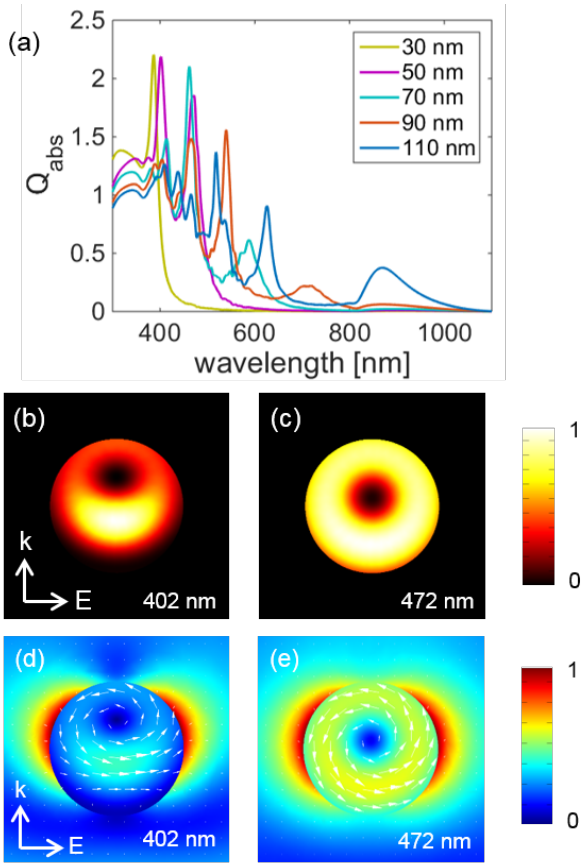

Fig. 1. (a) Absorption efficiencies of silicon nanospheres in water having different radii. (b-e) Cross sections of the simulated normalized absorption (b, c) and normalized electric field amplitude (d, e) in false color map for a 50-nm radius silicon nanosphere in water. Panels (b, d) and (c, e) are at 402 nm (second resonance) and 472 nm (first resonance), respectively. In the simulations, the incident light propagates from the bottom to the top and the electric field is polarized in horizontal direction.

3. Materials and methods

In experiment, we used silicon nanoparticles synthesized by thermal plasma method (Nisshin Engineering Inc.) [35]. Figure 2(a) shows the TEM image of the silicon nanoparticles (JEOL, JEM 2100F). All the particles look spherical. From the analysis of TEM images taken for 300 silicon nanoparticles, the particles size ranges from ~40 nm to ~250 nm in diameter and the average size of the particles is ~80 nm (see Fig. 6(a) in the Appendix). Dynamic light scattering (DLS) measurement was as well carried out (see Fig. 6(b)) and the average particle size from the DLS analysis is ~285 nm, indicating that some nanoparticles aggregated in water which were not large enough to sink down. The high-resolution TEM (HR-TEM) image (inset of Fig. 2(a)) confirms a single phase and pure silicon phase is evidenced by power XRD pattern (Rigaku, RINT 2000V/PC) shown Fig. 2(b). The d-spacing for the (111) peak obtained from the HR-TEM image is 0.313 nm, which matches well to the reference value [36].

Optical absorbance spectrum of the silicon nanofluid measured by an UV-VIS spectrometer (JASCO, V-570) is shown in Fig. 2(c). The measured spectrum is rather flat and

#253755 Received 10 Nov 2015; revised 22 Dec 2015; accepted 17 Jan 2016; published 27 Jan 2016

shows broad extinction from UV to NIR. This is due to the overlapping of the narrow absorption peaks of different sizes as shown in Fig. 1(a) and also confirmed by dark field microscopy (see Fig. 7 in the Appendix). A photograph of the silicon nanofuild at 0.001 vol% is shown in Fig. 2(d). As seen from the photo, the silicon nanoparticles dispersed very well in water.

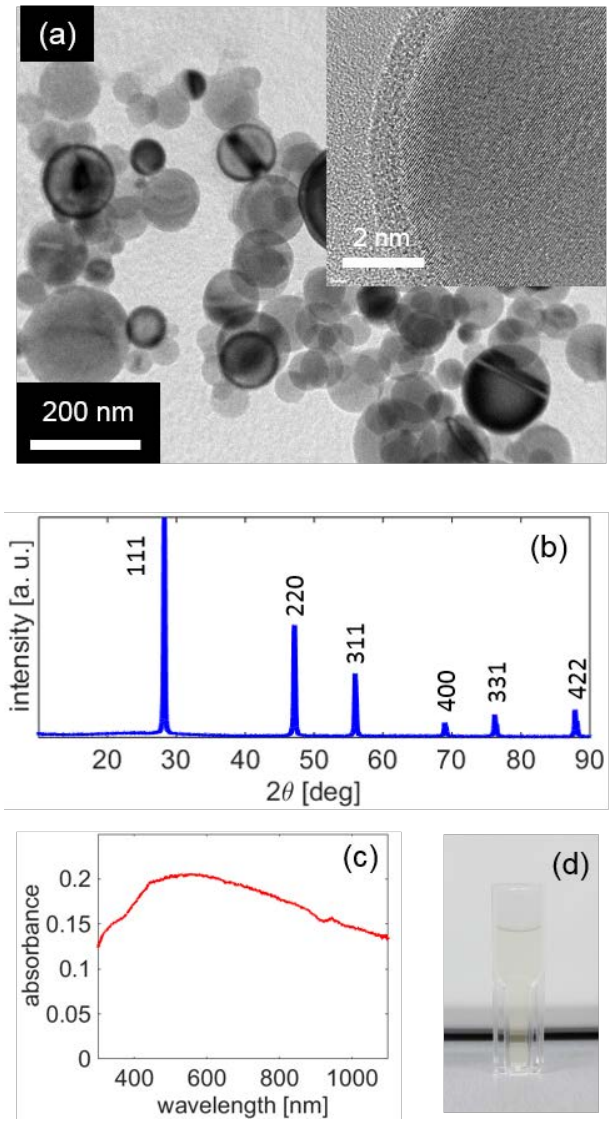

Fig. 2. (a) Bright field TEM image of the silicon nanoparticles. Inset shows the high-resolution TEM image. (b) Power XRD pattern of the silicon nanoparticles. (c) Extinction spectrum of the 0.001 vol% silicon nanoparticles in water in a 1-cm thick cell. The spectrum is normalized to pure water. (d) Photograph of silicon nanofluid at 0.001 vol%. The thickness of the plastic cell perpendicular direction to the photo is 1 cm.

To examine solar heating properties of the silicon nanoparticles due to sunlight absorption, the weighted silicon nanoparticles were dispersed in pure water and sonicated for a few minutes to form uniform mixture of silicon nanofluids as shown in Fig. 2(d). Three different concentrations of silicon nanofluids (20 mL each) were prepared in 50 mL beakers.

A commercial solar simulator (San-Ei Electronic, XES-40S1) was used as an artificial sunlight source to illuminate the nanofluids. During the measurements, the beaker containing

#253755 Received 10 Nov 2015; revised 22 Dec 2015; accepted 17 Jan 2016; published 27 Jan 2016

nanofluid was kept in a white plastic foam. The weight change due to evaporation of water and the temperature rise due to heating were measured by an electric balance (Shimadzu, AUW200D) and a K-type thermos-couple, respectively. The thermos-couple was placed at the bottom of the beaker. A photo of the experimental setup is shown in Fig. 8. The zero tracking function of the balance was disabled to measure minute weight changes. The weight changes were plotted after subtracting the natural evaporation at the room temperature. During the measurements, the room temperature and the humidity were kept at 21.4 ± 0.2 °C and 41 ± 1%, respectively.

4. Results and discussion

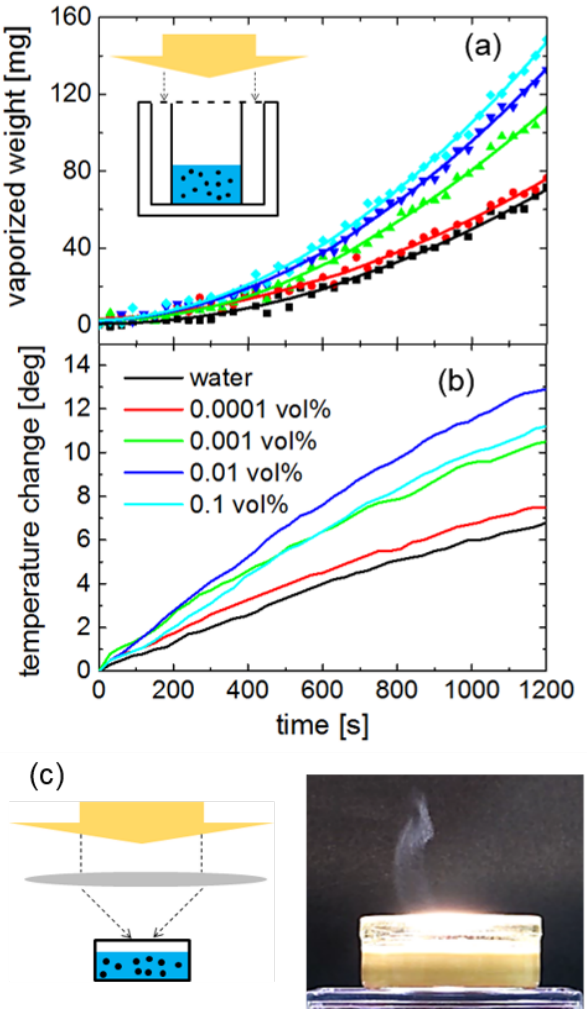

Fig. 3. Weight changes (a) and temperature changes (b) of the silicon nanofluids upon irradiation by a solar simulator. The legends for panel (a) is identical to panel (b). In panel (a), the measured data are represented by symbols and the solid lines are the fitted lines. The inset figure in panel (a) is a schematic of the setup and identical legends are used for panels (a) and (b). (c) Schematic of the setup with a focusing lens (left) and the photo of 0.1 vol% silicon nanofluid at the irradiation of ~800 mW/cm^2 from the solar simulator (right).

The weight losses and the temperature increases caused by the photothermal effect of silicon nanoparticles are shown in Figs. 3(a) and 3(b), respectively. These results were recorded at the irradiance of 80 mW/cm^2 without focusing. The vaporization rates are higher for higher

#253755 Received 10 Nov 2015; revised 22 Dec 2015; accepted 17 Jan 2016; published 27 Jan 2016

concentration nanofluids. After 1200 seconds, the vaporized weight for the 0.01 vol% nanofluid increased ~1.6 fold compared to pure water. The temperature increase rates are also higher for higher concentration and temperature increase of the 0.01 vol% nanofluid is 1.8 times higher than that of pure water. Both results indicate that silicon nanoparticles in water are playing a vital role to absorb sunlight and concentrate heat in the nanoscale to heat and vaporize water. Having these results, we define energy conversion efficiency (η) as, $\eta = (E_v + E_h)/E_{in}$, where E_v [J] and E_h [J] are the energies consumed to vaporize water and heat water, respectively, and E_{in} [J] is the energy of the sunlight which is incident on the opening of the white foam In contrast, the energy conversion efficiency of pure water was 29% at the identical setting. The efficiencies of the other nanofluids are tabulated in Fig. 9(c) in the Appendix. To exemplify the local heating of silicon nanoparticles, in Fig. 3(c) a photo of the silicon nanofluid is shown under the irradiation of focused sunlight at ~800 mW/cm^2. Even though the temperature of the nanofluid is well below the boiling temperature, steam is visible.

The results presented in Fig. 3 show great promise of using lossy Mie resonances of silicon nanoparticles for solar water heating and vaporization. The abundance and non-toxic property of silicon make silicon nanofluid attractive for practical applications. In the future, we anticipate that silicon nanofluid systems can replace conventional solar water heating systems and vapor generation from silicon nanofluid can be applied for water distillation.

5. Conclusion

To summarize, we show that silicon nanofluids show broadband absorption spectrum from UV to NIR covering more than 70 percent of the solar spectrum. Whereas each silicon nanoparticle has narrow absorption, our analytical calculation shows that an ensemble of silicon nanoparticles with various sizes is able to cover wide spectrum. The experiment with a solar simulator showed that silicon nanofluid can nearly double the vaporization and heating speeds compared to those of pure water. Our results indicate that silicon nanoparticles can be used to solar thermal applications such as solar water heating and water distillation.

Appendix

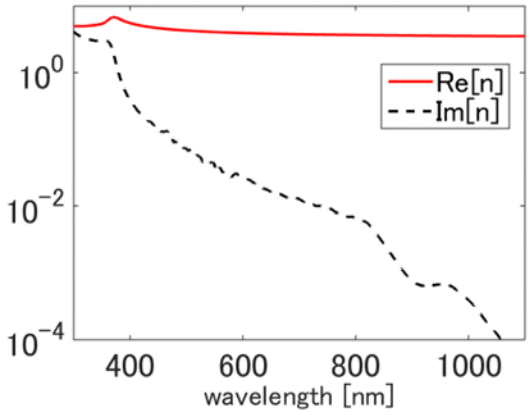

Fig. 4. Complex refractive index of silicon [27].

#253755 Received 10 Nov 2015; revised 22 Dec 2015; accepted 17 Jan 2016; published 27 Jan 2016

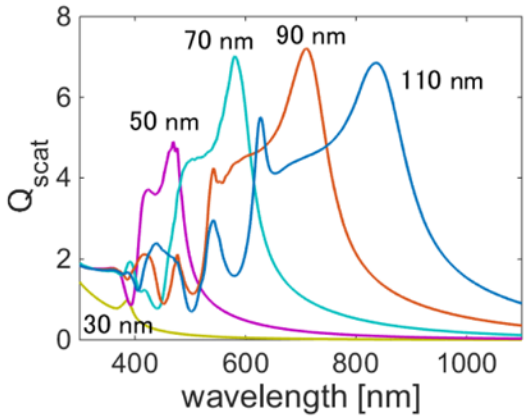

Fig. 5. Scattering efficiencies (Q_{scat}) of silicon nanospheres in water having different radii. The refractive index of silicon is taken from ref [27].

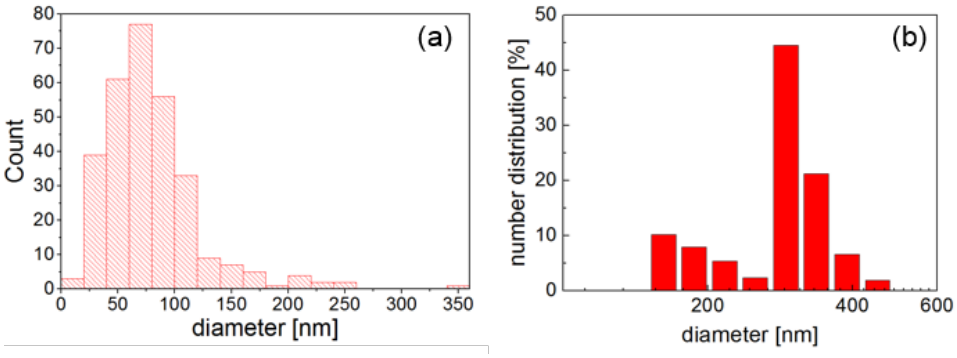

Fig. 6. (a) Size distribution of the silicon nanoparticles measured from the TEM images showing 300 particles in total. (b) Histogram of the silicon nanoparticle diameter in water by DLS measurement.

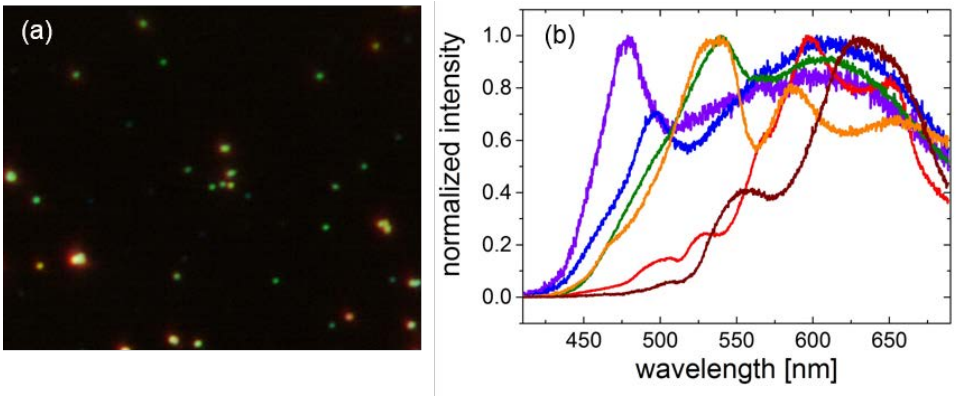

Fig. 7. (a) Dark field microscope image of the silicon nanoparticles on a cover glass. Different colors correspond to different sizes of the silicon nanoparticles. (b) Selected spectra of the backward scattering from the silicon nanoparticles on a cover glass. Each spectrum is normalized to its maximum.

#253755 Received 10 Nov 2015; revised 22 Dec 2015; accepted 17 Jan 2016; published 27 Jan 2016

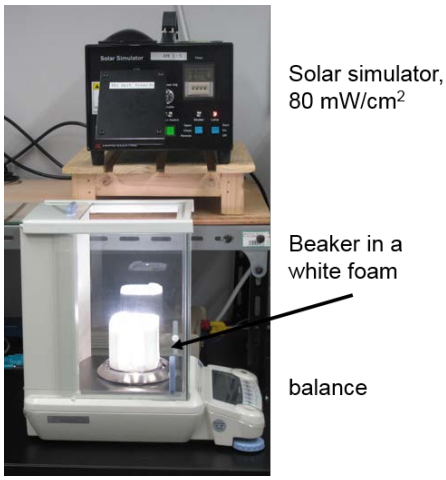

Fig. 8. Photograph of the measurement setup when the solar simulator is on.

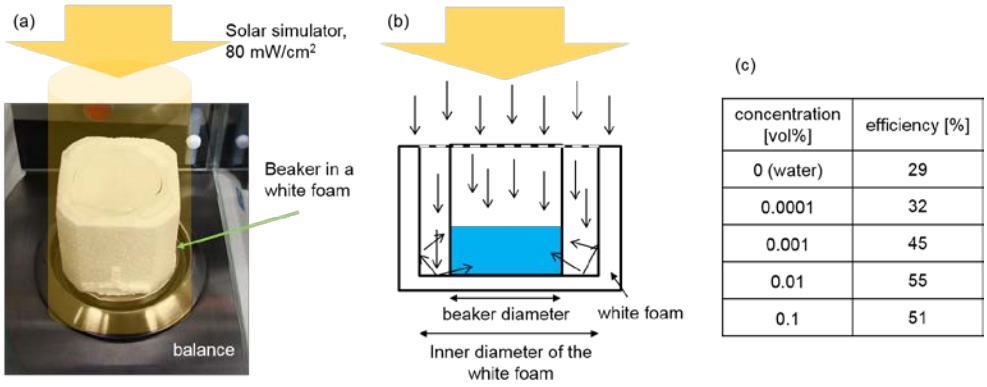

(c)

concentration [vol%]	efficiency [%]
0 (water)	29
0.0001	32
0.001	45
0.01	55
0.1	51

Fig. 9. (a) Photo of the experimental setup and (b) schematic drawing of the cross section of the setup. The thermos-coupler was removed when taking the photo. The beam size of the solar simulator was larger than the cross section of the white foam. Since the surface of the white foam is rough, scattered light can illuminate the nanofluid from the side. (c) Efficiencies of the silicon nanofluids.

Acknowledgements

This work is partially supported by the JSPS KAKENHI Grant Number 15K17447.

#253755 Received 10 Nov 2015; revised 22 Dec 2015; accepted 17 Jan 2016; published 27 Jan 2016